Hindawi Publishing Corporation
Journal of Nanomaterials
Volume 2008, Article ID 948183, 8 pages
doi:10.1155/2008/948183

Research Article

Electrode Properties of Mn_2O_3 Nanospheres Synthesized by Combined Sonochemical/Solvothermal Method for Use in Electrochemical Capacitors

Teressa Nathan, Michael Cloke, and S. R. S. Prabaharan

Faculty of Engineering, The University of Nottingham Malaysia Campus, Jalan Broga, Semenyih 43500, Malaysia

Correspondence should be addressed to S. R. S. Prabaharan, prabaharan.sahaya@nottingham.edu.my

Received 17 October 2008; Accepted 28 December 2008

Recommended by Sang-Hee Cho

We report here an efficient single step combined sonochemical and solvothermal synthesis process to obtain bulk quantities of nanospherical particles of cubic Mn_2O_3 and characterized its pseudocapacitive characteristics in relevance to electrochemical capacitors for the first time. It has been found that quantitative determination of specific capacitance yielded a value of capacitance of $\sim 100\,Fg^{-1}$ within 0–0.4 V (versus SCE) potential range in a 6 M KOH alkaline electrolyte. The as-prepared nanopowders after being subjected to heat treatment at 400°C were characterized by using XRD which shows a typical cubic single-phase structure (space group *Ia-3*), the broad crystalline peaks indicating the presence of explicit nanostructure. Electron microscopic studies (FE-SEM and TEM) revealed that the synthesized powders exhibit nanospherical morphology with uniform sphere-like grains of ~10–15 nm range. Two heat-treated samples were studied in the context of crystallinity versus electrochemical capacitance using rate-dependent cyclic voltammetry (CV) and electrochemical impedance spectroscopy (EIS) in a three-electrode system. The excellent well-refined redox behavior corroborates with EIS measurements. The presence of near symmetric redox couple observed in CV has been attributed to pronounced one-electron-transfer process owing to the presence of facile Mn redox centere facilitating the reversible one-electron transfer that accounts for its pseudocapacitance.

1. INTRODUCTION

Although the concept of electrochemical capacitor was initialized and industrialized almost 40 years ago, the demand for high power pulse requirements in today's modern power hunger electrical and electronic devices such as telecommunication devices (mobile phones, PDA, etc.) standby power systems, memory protection of computer electronics, and hybrid electric vehicles in the form of storage components rendered a renewed interest in electrochemical capacitors (ECs). Depending on their charge storage mechanism, ECs utilize both nonfaradic and faradic capacitance, namely, electrochemical double-layer capacitance (EDLC) and pseudocapacitance, respectively. The origin of capacitance in the EDLC is charge separation at the electrode-electrolyte interface, whereas pseudocapacitance arises from fast, reversible faradic redox reactions taking place in the bulk of electrodes. The capacitance in an EDLC is in the order of tens and in the pseudocapacitor, it is in the order of hundreds of μF per cm^2 of interfacial area [1]. The materials being studied for EC applications are mainly three types: carbons [2, 3], metal oxides [4–6], and electronically conducting polymers [7]. In the first type, high-surface-area carbon materials (activated carbon black, carbon aerogel, and carbon nanotubes) are used as symmetric electrodes to form electrochemical double-layer capacitors (EDLCs) in which the charge storage is a result of electrostatic charge separation at the interface between the electrode and the electrolyte. Specific capacitance of 280 and $120\,Fg^{-1}$ can be achieved in aqueous and nonaqueous electrolytes with the maximum voltages of 1 and ~3 V, respectively [8]. On the other hand, the above type-II and type-III category of materials possess both Faradic charge transfer reaction (battery-like) and non-diffusional charge reaction (capacitor-like) characteristics, together with high bulk electronic conductivity. It has been demonstrated that even higher capacitance can be achieved by using these redox-active materials. These materials store electrochemical charge using highly reversible surface redox

reactions, commonly described as *pseudocapacitance* in the literature. The introduction of these fast, reversible surface processes has drastically increased the charge-storage performance. Amongst type-II category, hydrous ruthenium oxide was reported as the most promising material with specific capacitance values as high as 863 Fg^{-1} [9]. Though noble metal oxides or hydrous oxides yield remarkably large value of capacitance, the high cost of these materials precludes their application. On the other hand, conducting polymer-based electrochemical capacitors represents an interesting class, thanks to the combination of high capacitive energy density and low material cost [10–12]. However, conducting polymer-based materials also have some disadvantages that include lower cycle life and slow kinetics of ion transport because the redox sites in the polymer backbone are not sufficiently stable for many repeated redox processes [13, 14]. Hence, it is extremely important to develop alternative electrode materials with a combination of low cost and improved performances.

Amongst many transition metal oxides being investigated for EC applications, manganese oxides emerge as potential candidates for many niche applications (high power batteries, chemical sensing devices, catalysts electronics, etc.) in terms of cost and environmentally benign qualities. As far as the chemical valence states of manganese oxide are concerned, it possesses different oxidation states (2+, 3+, 4+, and 6+). Amongst them, MnO_2 is one of the common manganese oxide phases which are extensively investigated because of its applications as catalysts in ion sieves, as electrode materials in primary Li/MnO_2 batteries as well as in electrochemical capacitors [15–21]. The preparation of MnO_2 requires stringent procedures owing to its complicated means of process control. There have been many synthesis methods adapted for MnO_2 such as chemical coprecipitation [22], thermal oxidation [23], sol-gel [24], and improved reduction process [25]. In the context of electrochemical capacitors, manganese oxide phases occupied a place of pride in the recent past. Over the years, researchers reported various specific capacitance values for MnO_2 in the open literature [26, 27].

As far as manganese oxide phases are concerned, the most common phases of manganese oxide in air at different temperatures are shown below. That is, the following thermal oxidation reactions are possible in manganese oxides [28]. It is well known that MnO_2 exhibits thermochemical changes as shown below,

$$MnO_2 \xrightarrow{500^\circ C} Mn_2O_3 \xrightarrow{900^\circ C} Mn_3O_4 \xrightarrow{1700^\circ C} MnO. \quad (1)$$

Amongst different phases of manganese oxide, Mn_2O_3 possesses poor electronic conductivity. Nevertheless, its pronounced electrochemical redox activity via Mn^{3+} to Mn^{4+} transition giving rise to one electron transfer. The diminished electron transfer reaction, though significant from the point of view of electrode reaction in ECs, is still an unexplored material for pseudocapacitance applications until Nathan and Fauzi [29] demonstrated recently that Mn_2O_3 could be regarded as a capacitor material that possesses significant pseudocapacitive characteristics. Even though, the quantum of energy associated with one electron transfer is limited; it is believed that cubic phase of Mn_2O_3 makes it possible to be used as a pseudocapacitance electrode in ECs.

In the present study, we report here for the first time the synthesis of Mn_2O_3 nanospheres employing a novel solvothermal/ultrasonication, a modified single step synthesis protocol from the one described by us previously [30]. Using the rate-dependent cyclic voltammetry, a single electrode pseudocapacitance behavior of Mn_2O_3 nanosphere electrodes has been studied using a three-electrode cell comprised of a platinum counter and SCE as reference electrodes in alkaline medium (6 M KOH).

2. EXPERIMENTAL DETAILS

2.1. Synthesis of nanospherical manganese oxide

The nanospherical Mn_2O_3 is a direct product of the soft-combustion of $Mn(NO_3)_2 \cdot 4H_2O$ with citric acid and acetone/isopropanol solvent mixture. A 0.1 M aqueous solution of $Mn(NO_3)_2$ was prepared using deionised water. The solution was thoroughly mixed with varying amounts of citric acid and acetone/isopropanol and subjected to sonication (Ultrasonic processor, UP200S, 200 watts, 24 kHz, Hielscher, Germany) at ambient conditions with a high-density ultrasonic Ti probe immersed directly in the solution. During the ultrasonic irradiation, the temperature of the reaction solution rose to ~80°C and the ultrasonic irradiation was continued to be maintained at this temperature for 20 minutes. It is a similar method (without sonication) that was previously reported by us to synthesize nanostructured NiO powders of 10–15 nm size [30]. In the present synthesis protocol, citric acid was introduced as a chelating agent which induces molecular level mixing by dissociating the ionic species of the starting material, while acetone/isopropanol mixture acts as a handle to promote nonhydrolytic condensation of $Mn(NO_3)_2$ dissolute. The solution remained clear throughout the process without forming any turbid solution (no precipitation) as it was gently stirred at 70°C for 1 hour in ambient conditions until all the solvents were evaporated, leaving a wet gel-like substance, the so-called precursor. As the precursor is further heated up to 350°C, the wet gel-like substance turns into a brownish paste, releasing brown-colored fumes as a result of the ignition of organic moieties and finally yielding the as-prepared final product. Postannealing was carried out at 400°C for 1 hour and 5 hours to study the grain growth and structural stability and to ensure the structural perfection so as to obtain the electrode-active characteristics.

As described Mn_2O_3 nanoparticles were obtained via a combined solvothermal/ultrasonication technique in which the precursor solution was obtained after the ultrasonic irradiation of the initial phase of precursor preparation. The presence of citric acid (chelating agent) facilitated the complexation by modifying ligands in the original precursor solution slows down the pace of hydrolysis and condensation. Citric acid is the widely being used as a complexing agent for solution-based solvothermal methods

for preparing electrode-active transition metal oxides [30]. Citric acid (H3L) is a weak triprotic acid which dissociates in a stepwise manner in the solution depending upon the solution pH; only when the pH value of the solution is >6, the species L becomes the dominant one [31]. The complexation reactions between metal ions and citric acid are also highly dependent upon the pH of the solution and cannot occur, in general, in a very strong acidic solution. However, we did not alter the pH of the total solution as it is the mixture solution that quickly forms a clear solution (without adding ammonia water) upon ultrasonication. Sonochemical reactions are often explained by means of cavitation collapse or microjet [32]. The chemical effect of ultrasound arises from acoustic cavitation phenomena such as formation, growth, and implosive collapse of bubbles in a liquid medium [33]. The initial reduction of the starting material was facilitated by both the temperature and the sonication followed by the reaction of chelating agent. Thus, we suggest that citric acid coordinated to Mn ions in $Mn(NO_3)_2$ methanolic solution, making the nucleation complete at the early stage of the solvothermal process and inhibiting the crystal growth.

2.2. Mn_2O_3 composite electrode preparation

The Mn_2O_3 composite electrode was prepared by using a well-known procedure previously reported [30]. The composite electrodes were fabricated by forming the slurry comprising of a mixture of Mn_2O_3/polyvinylidene fluoride (PVdF)/acetylene black in 80:10:10 ratio, respectively, and by stirring it for 30 minutes. Acetylene black (AB) was added to increase the conductivity of the Mn_2O_3 powders. The thick slurry was then coated on a stainless steel expanded mesh (EXMET, CT, USA) and dried in a vacuum oven at 70°C overnight to eliminate any residual moieties. The dried pellets were cut into a 4 cm^2 area circular disk-like composite electrodes and used as a working electrode in a three-electrode cell in which a platinum foil was used as a counter electrode employing an aqueous electrolyte (6 M KOH) against standard calomel electrode (SCE). The rate-dependent cyclic voltammetry was performed between the potential range of 0 up to 0.4 V versus SCE in the above three-electrode cell.

2.3. Physical and electrochemical characterization

The crystallographic phase of the annealed products of Mn_2O_3 (400°C/1 hour and 5 hours in air) was confirmed by powder X-ray diffraction (XRD) using a Siemens diffractometer D5000 using CuKα radiation (λ = 0.154056 nm). Nanostructure morphology of the annealed product was observed under field-emission scanning electron microscopy (FE-SEM, JEOL JSM-6701F, Tokyo, Japan) incorporating a cold cathode field emission gun, equipped with a conical FE gun and a semi-in-lens electron optics. TEM analysis was carried out using a Philips CM 12(s) TEM to determine the particle size. No coating was done prior to analysis and images were obtained on the as-synthesized powders, prior to loading. The rate-dependent cyclic voltammetry and ac impedance measurements were carried out using a PAR VersaSTAT^3 Potentiostat/Galvanostat (Ametek, Pa, USA) equipped with V3-Studio software for data acquisition and analysis.

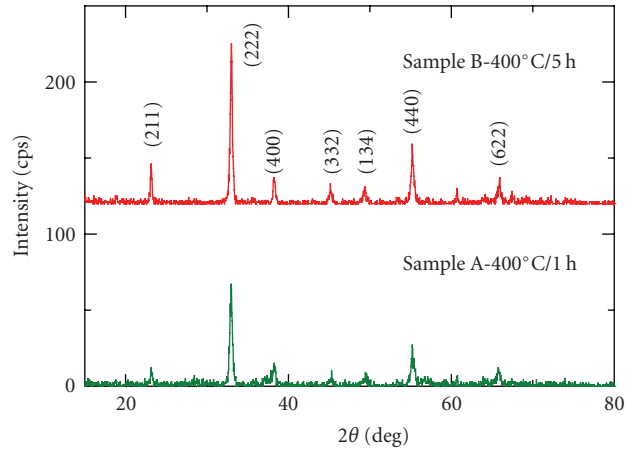

FIGURE 1: X-ray diffractograms of Mn_2O_3 showing broad crystalline peaks; sample A heated at 400°C for 1 hour and sample B heated at 400°C for 5 hours.

3. RESULTS AND DISCUSSION

3.1. Structural and microstructural (nanophase) characterization of the active electrode material, Mn_2O_3

A single-phase cubic structure of Mn_2O_3 was evident from XRD analysis as shown in Figure 1. The *hkl* planes are well-indexed to a cubic phase with lattice parameter a = 9.4080 Å having broad crystalline peaks indicating the presence of explicit nanostructure. Obviously, the broad peaks illustrate the presence of small crystallites (domains) and by knowing the FWHM peak information from the powder diffraction data, the particle size of the crystallites can be estimated by using Scherrer's formula. The structural results are in good agreement with the JCPDS 41-1442 database. The effect of postheat treatment versus time has been investigated in order to study the electrode-active Mn_2O_3 nanospheres. Figure 1 shows the XRD pattern obtained on a sample annealed at 400°C for 1 hour and 5 hours as holding time. As the holding time is increased from 1 hour to 5 hours (*sample A* and *sample B*, resp.), while maintained at 400°C, XRD peaks became relatively sharper yet maintaining the features corresponding to its nanostructure (broad crystalline peaks).

TEM images on the annealed samples are reproduced in Figure 2. Figure 2(a) reveals that the manganese oxide powders synthesized at 400°C exhibit spherical-shaped particles (within 10–15 nm range) with porous morphology. The spherical shape of the product was also ascertained by FE-SEM analysis as well. It has been found that as the annealing time increased to 5 hours, the particle size remains the same and possible grain growth is not explicitly evident as shown

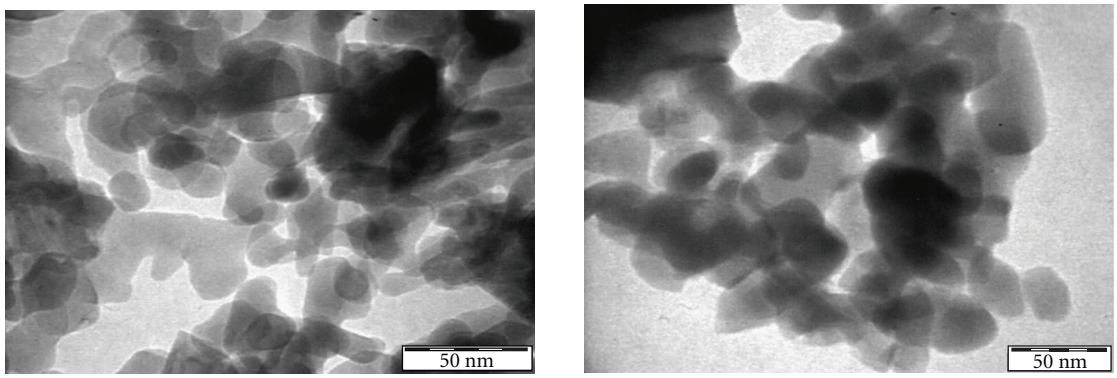

(a) (b)

Figure 2: TEM pictures of Mn_2O_3 heated at 400°C for (a) 1 hour and (b) 5 hours.

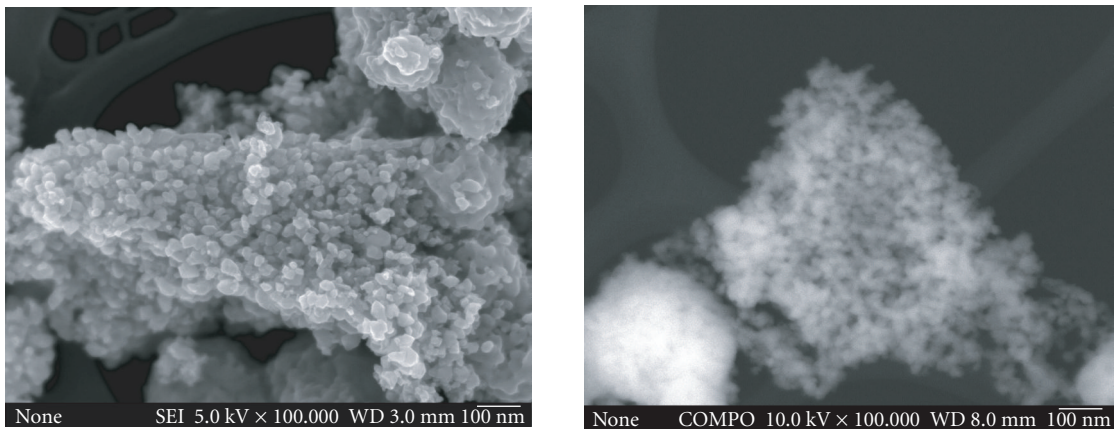

(a) (b)

Figure 3: Nanosphere Mn_2O_3 heated at 400°C for 5 hours (a) FE-SEM image and (b) Back scattered image.

in Figures 3(a) and 3(b). The porous particle morphology was evident from the FESEM analysis.

3.2. Electrochemical characteristics of Mn_2O_3 nanospheres

3.2.1. Electrochemical impedance spectroscopy analysis: single electrode characteristics

Figure 4 shows the *ac* impedance plots of the Mn_2O_3 electrodes of *samples A* and *B* in 6 M KOH electrolyte measured at OCV of ca. 0.4 V versus SCE with a frequency range of 10^5–10^{-2} Hz with an applied 20 mV peak to peak sinusoidal perturbation voltage. As seen in Figure 4, the frequency dispersion over the complex impedance plot is composed of a small solution resistance followed by a semicircle at the mid frequency region and ~45° spike accompanied by a straight line. The semicircle at higher frequency region is possibly attributed to the charge transfer process at electrode/electrolyte interface, and 45° the straight line at lower frequency region should be ascribed to the diffusion process in solid. It can be seen from Figure 4 that the semicircle for *sample A* is a little smaller than that of *sample B*. This suggests that the electrochemical reaction resistance in *sample A* is smaller comparatively. In addition, the straight line at the lower frequency region for *sample A* is less inclined than that of *sample B*, suggesting that the former is less capacitive than the later. Alternatively, one can think of the possible surface roughness factor causing this depression at the double-layer frequency response regime. Nevertheless, our interpretation of the effect of depression at low-frequency regime for both samples corroborates with our CV results. From the impedance data at the lower frequency region, it can be seen that at the same frequency regime, the values of the real and the imaginary impedances and thus the overall impedance of *sample A* are smaller than that of *sample B*, suggesting that the latter has a smaller solid-state diffusion impedance at the interface with the electrolyte and a larger capacitance. Considering the little difference in the charge transfer resistance (semicircle portion) at higher frequency region, the EIS results are corroborated with the cyclic voltamograms as shown in Figure 5.

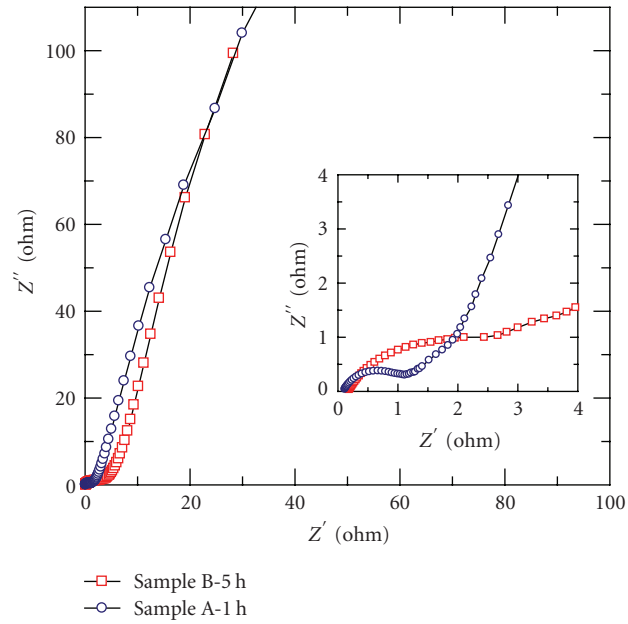

FIGURE 4: *ac* impedance plots of the Mn_2O_3 electrodes of sample A and B in 6 M KOH electrolyte measured at OCV (0.4 V versus SCE) within a frequency range of 10^5–10^{-2} Hz.

3.2.2. *Rate-dependent cyclic voltammetry (CV): single electrode properties*

The pseudocapacitive behavior of the synthesized manganese oxide was examined by a cyclic voltammetry technique at different scan rates. Mn_2O_3 heated at 400°C, which was coated on a stainless steel expanded mesh, was later used as a working electrode in a three-electrode electrochemical cell, and the electrode potential was scanned between 0.0 and 0.4 V versus SCE in both anodic and cathodic directions. The rate-dependent current responses were measured at different scan rates from 5 mVs^{-1} up to 100 mVs^{-1} as shown in Figure 5. Figures 5(a) and 5(b) depict the voltammograms recorded for sample A (Mn_2O_3 heated at 400°C/1 h) and sample B (Mn_2O_3 heated at 400°C/5 h) at various scan rates, respectively.

The electrochemical reaction of Mn_2O_3 in alkaline solution has not been discussed much in the literature according to our knowledge. Recently, Lin et al. described a sol-gel manganese oxide with Mn_2O_3 and Mn_3O_4 mixture, suggesting that the relatively low valence states of $Mn^{2.67+}$ (Mn_3O_4) and Mn^{3+} (Mn_2O_3) changed into high valence Mn^{4+} after cyclic voltammetry [34]. That is, its pseudocapacitance is known to arise from electron transfer at the Mn sites, and the charge transfer was thought to be balanced either by chemisorption/desorption of electrolyte cations [35] or by insertion/deinsertion of protons [16] as shown in the equation

$$MnO_2 + H^+ + e^- \longrightarrow MnOOH. \quad (2)$$

However, in a recent report it was suggested that the reaction involves bulk insertion/extraction of both oxonium

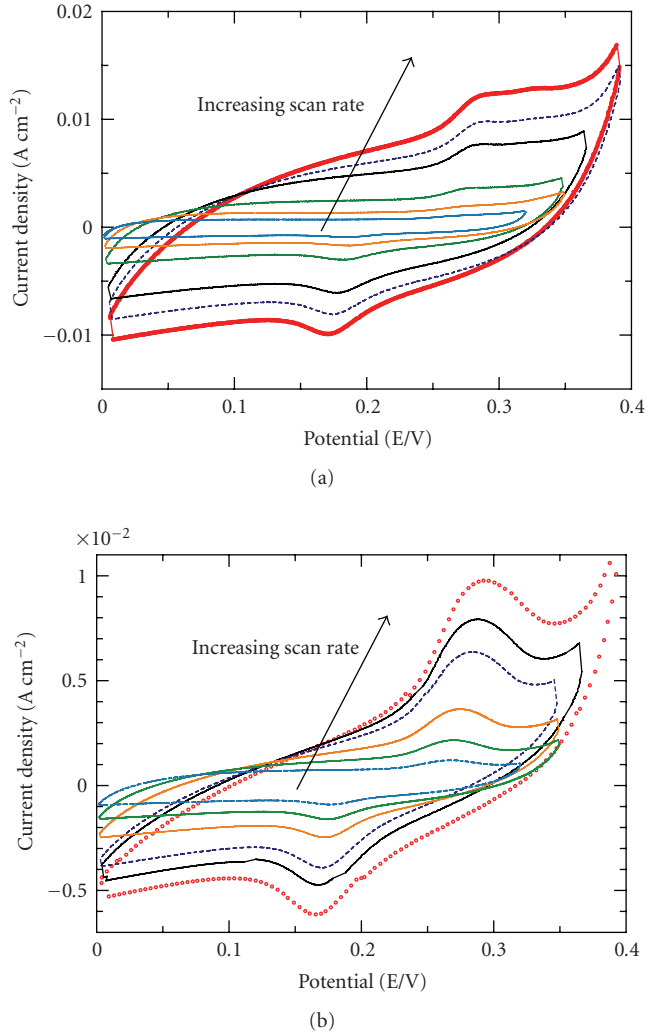

FIGURE 5: Cyclic voltammograms of sample A (Mn_2O_3 heated at 400°C/1 h) and sample B (Mn_2O_3 heated at 400°C/5 h) at different scan rates. Arrow indicates increasing scan rate (100, 70, 50, 20, 10, and 5 mVs^{-1}).

(H_3O^+) and electrolyte cation as confirmed by electrochemical quartz-crystal microbalance (EQCM) and in-situ XAS analysis [36].

As far as Mn_2O_3 is concerned, Mn^{3+} in Mn_2O_3 is reasonably described as going through an oxidation reaction giving rise to one electron transfer attaining a valence state of Mn^{4+}. Accordingly, the CV profiles of composite Mn_2O_3 electrode versus SCE are not perfectly rectangular but exhibit near symmetric redox humps between 0 and 0.4 V. As shown in Figure 6, well-resolved oxidation and reduction peaks are evident at about 0.27 V and 0.17 V, respectively, during the charge/discharge reaction. However, *sample A* shows no clear oxidation peak unlike *sample B*. The latter showed well-resolved redox peaks presumably due to facile crystal structure caused by prolonged annealing of the sample. The extended holding time could probably help in attaining the facile cubic structure as confirmed by the well-resolved diffraction peaks in Figure 1.

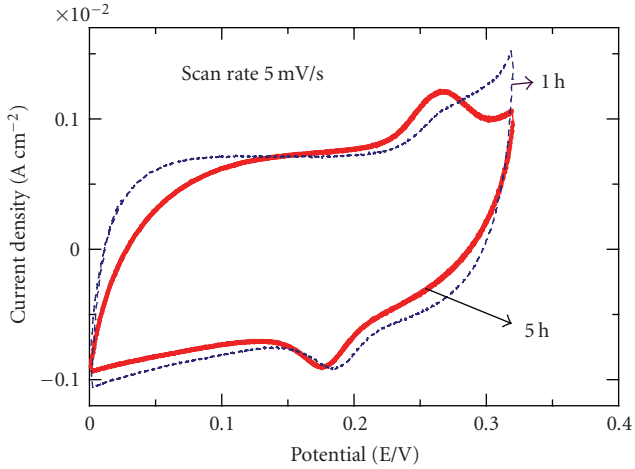

FIGURE 6: Cyclic voltammograms of nanostructured Mn_2O_3 (annealed at 400°C for 1 h and 5 h) as working electrode against SCE in a three electrode cell at 5 mV/s.

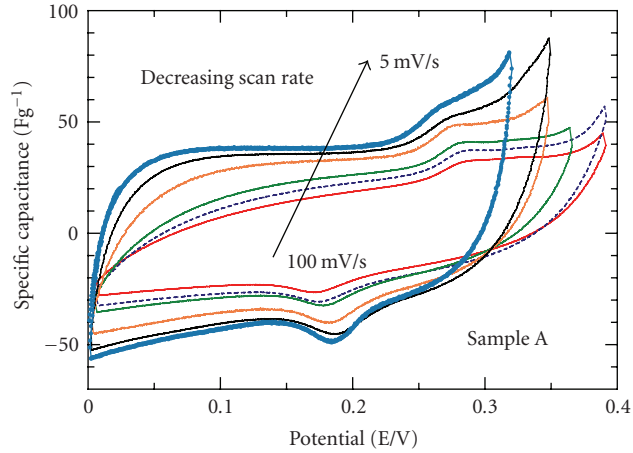

(a)

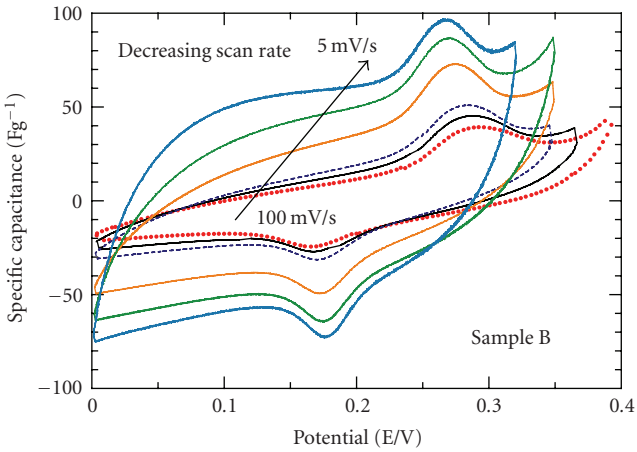

(b)

FIGURE 7: Specific capacitance versus potential plot of nanospherical Mn_2O_3. Arrow indicates decreasing scan rate (100, 70, 50, 20, 10, and 5 mVs^{-1}).

This facilitates the easy reaction kinetics of OH^- being chemisorbed and/or intercalated into host Mn_2O_3 cubic lattice. Accordingly, the following electrochemical reaction is expected to take place during the charge/discharge process involving OH^- chemisorption/intercalation into Mn_2O_3 structure:

$$\mathrm{Mn[Mn]O_3 + OH^- \underset{\text{Discharge}}{\overset{\text{Charge}}{\rightleftharpoons}} Mn^{4+}[Mn^{3+}]OH^-O_3 + e^-}. \tag{3}$$

The average specific capacitance versus voltage for Mn_2O_3 deduced using the formula

$$C_{\text{specific}} = \frac{i}{sw}, \tag{4}$$

where i is the instantaneous current, s is the potential scan rate, and w is the mass of the active material in an electrode. Accordingly, a specific capacitance of 40–50 Fg^{-1} has been obtained for sample A at 5 mVs^{-1} scan rate (see Figure 7).

As expected, *sample B* rendered almost twice the capacitance 90–100 Fg^{-1} at 5 mVs^{-1}. One plausible cause for the lower specific capacitance is probably the existence of Mn^{3+} oxidation state of Mn in Mn_2O_3. This has probably resulted in diminished specific capacitance. Also, there is another possible reason related to the presence of two distinct Mn atom sites in Mn_2O_3 [37]; Mn^{3+} partially occupies octahedral site as well as distorted octahedral site. Perhaps this may have caused a portion of Mn ion present in Mn_2O_3 to be partially not available in the electrochemical oxidation reaction. Obviously, such hindrances might diminish the specific capacitance even further. The studies on hybrid asymmetric capacitor employing nanosphere Mn_2O_3 as positive electrode against a mesoporous carbon negative electrode will be reported elsewhere.

4. CONCLUSION

An efficient simple synthesis protocol has been reported to synthesize nanospherical manganese oxide, Mn_2O_3 (grain size within 10–15 nm), by means of a simple combined solvothermal/ultrasonication at low temperature. The nanostructure features have been confirmed by both XRD and electron microscopic analysis (FE-SEM and TEM). The rate-dependent cyclic voltammetry revealed that both Mn_2O_3 samples exhibit redox reaction via Mn^{3+}/Mn^{4+} couple yielding one electron transfer which corresponds to the electrochemical capacitance of ~100 Fg^{-1} in alkaline medium (6 M KOH). The modest specific capacitance has been attributed to the presence of facile crystal structure facilitating the easy insertion/removal of electrolyte ions (OH^-) in Mn_2O_3 nanospheres. The EIS measurements also corroborate the findings of CV results with respect to heat-treated samples as a function of holding time (*sample A and sample B*).

ACKNOWLEDGMENTS

S. R. S. Prabaharan would like to thank the Ministry of Science, Technology and Innovation (MOSTI, Malaysia) for financial support through Project no. 03-02-12-SF0011. T. Nathan thanks MOSTI for research assistantship (RA).

REFERENCES

[1] C. Lin, J. A. Ritter, and B. N. Popov, "Development of carbon-metal oxide supercapacitors from sol-gel derived carbon-ruthenium xerogels," *Journal of the Electrochemical Society*, vol. 146, no. 9, pp. 3155–3160, 1999.

[2] H. Nakagawa, A. Shudo, and K. Miura, "High-capacity electric double-layer capacitor with high-density-activated carbon fiber electrodes," *Journal of the Electrochemical Society*, vol. 147, no. 1, pp. 38–42, 2000.

[3] E. Frackowiak and F. Béguin, "Carbon materials for the electrochemical storage of energy in capacitors," *Carbon*, vol. 39, no. 6, pp. 937–950, 2001.

[4] P. Novák, K. Müller, K. S. V. Santhanam, and O. Haas, "Electrochemically active polymers for rechargeable batteries," *Chemical Reviews*, vol. 97, no. 1, pp. 207–281, 1997.

[5] Y. U. Jeong and A. Manthiram, "Amorphous tungsten oxide/ruthenium oxide composites for electrochemical capacitors," *Journal of the Electrochemical Society*, vol. 148, no. 3, pp. A189–A193, 2001.

[6] L. Cao, L.-B. Kong, Y.-Y. Liang, and H.-L. Li, "Preparation of novel nano-composite $Ni(OH)_2$/USY material and its application for electrochemical capacitance storage," *Chemical Communications*, vol. 10, no. 14, pp. 1646–1647, 2004.

[7] Y.-K. Zhou, B.-L. He, W.-J. Zhou, and H.-L. Li, "Preparation and electrochemistry of SWNT/PANI composite films for electrochemical capacitors," *Journal of the Electrochemical Society*, vol. 151, no. 7, pp. A1052–A1057, 2004.

[8] I. Tanahashi, A. Yoshida, and A. Nishino, "Electrochemical characterization of activated carbon-fiber cloth polarizable electrodes for electric double-layer capacitors," *Journal of the Electrochemical Society*, vol. 137, no. 10, pp. 3052–3057, 1990.

[9] H. Kim and B. N. Popov, "Characterization of hydrous ruthenium oxide/carbon nanocomposite supercapacitors prepared by a colloidal method," *Journal of Power Sources*, vol. 104, no. 1, pp. 52–61, 2002.

[10] E. Frackowiak, K. Jurewicz, S. Delpeux, and F. Béguin, "Nanotubular materials for supercapacitors," *Journal of Power Sources*, vol. 97-98, pp. 822–825, 2001.

[11] A. Rudge, I. Raistrick, S. Gottesfeld, and J. P. Ferraris, "A study of the electrochemical properties of conducting polymers for application in electrochemical capacitors," *Electrochimica Acta*, vol. 39, no. 2, pp. 273–287, 1994.

[12] D. Bélanger, X. Ren, J. Davey, F. Uribe, and S. Gottesfeld, "Characterization and long-term performance of polyaniline-based electrochemical capacitors," *Journal of the Electrochemical Society*, vol. 147, no. 8, pp. 2923–2929, 2000.

[13] J. H. Park, J. M. Ko, O. O. Park, and D.-W. Kim, "Capacitance properties of graphite/polypyrrole composite electrode prepared by chemical polymerization of pyrrole on graphite fiber," *Journal of Power Sources*, vol. 105, no. 1, pp. 20–25, 2002.

[14] J. H. Park, O. O. Park, K. H. Shin, C. S. Jin, and J. H. Kim, "An electrochemical capacitor based on a $Ni(OH)_2$/activated carbon composite electrode," *Electrochemical and Solid-State Letters*, vol. 5, no. 2, pp. H7–H10, 2002.

[15] H. Y. Lee and J. B. Goodenough, "Supercapacitor behavior with KCl electrolyte," *Journal of Solid State Chemistry*, vol. 144, no. 1, pp. 220–223, 1999.

[16] S.-C. Pang, M. A. Anderson, and T. W. Chapman, "Novel electrode materials for thin-film ultracapacitors: comparison of electrochemical properties of sol-gel-derived and electrodeposited manganese dioxide," *Journal of the Electrochemical Society*, vol. 147, no. 2, pp. 444–450, 2000.

[17] Y. U. Jeong and A. Manthiram, "Nanocrystalline manganese oxides for electrochemical capacitors with neutral electrolytes," *Journal of the Electrochemical Society*, vol. 149, no. 11, pp. A1419–A1422, 2002.

[18] J.-K. Chang and W.-T. Tsai, "Material characterization and electrochemical performance of hydrous manganese oxide electrodes for use in electrochemical pseudocapacitors," *Journal of the Electrochemical Society*, vol. 150, no. 10, pp. A1333–A1338, 2003.

[19] C.-C. Hu and C.-C. Wang, "Nanostructures and capacitive characteristics of hydrous manganese oxide prepared by electrochemical deposition," *Journal of the Electrochemical Society*, vol. 150, no. 8, pp. A1079–A1084, 2003.

[20] H. Y. Lee, S. W. Kim, and H. Y. Lee, "Expansion of active site area and improvement of kinetic reversibility in electrochemical pseudocapacitor electrode," *Electrochemical and Solid-State Letters*, vol. 4, no. 3, pp. A19–A22, 2001.

[21] M. Toupin, T. Brousse, and D. Bélanger, "Charge storage mechanism of MnO_2 electrode used in aqueous electrochemical capacitor," *Chemistry of Materials*, vol. 16, no. 16, pp. 3184–3190, 2004.

[22] T. E. Moore, M. Ellis, and P. W. Selwood, "Solid oxides and hydroxides of manganese," *Journal of the American Chemical Society*, vol. 72, no. 2, pp. 856–866, 1950.

[23] J. W. Long, A. L. Young, and D. R. Rolison, "Spectroelectrochemical characterization of nanostructured, mesoporous manganese oxide in aqueous electrolytes," *Journal of the Electrochemical Society*, vol. 150, no. 9, pp. A1161–A1165, 2003.

[24] R. N. Reddy and R. G. Reddy, "Sol-gel MnO_2 as an electrode material for electrochemical capacitors," *Journal of Power Sources*, vol. 124, no. 1, pp. 330–337, 2003.

[25] S.-J. Bao, B.-L. He, Y.-Y. Liang, W.-J. Zhou, and H.-L. Li, "Synthesis and electrochemical characterization of amorphous MnO_2 for electrochemical capacitor," *Materials Science and Engineering A*, vol. 397, no. 1-2, pp. 305–309, 2005.

[26] T. Xue, C.-L. Xu, D.-D. Zhao, X.-H. Li, and H.-L. Li, "Electrodeposition of mesoporous manganese dioxide supercapacitor electrodes through self-assembled triblock copolymer templates," *Journal of Power Sources*, vol. 164, no. 2, pp. 953–958, 2007.

[27] A. S. Aricò, P. Bruce, B. Scrosati, J.-M. Tarascon, and W. van Schalkwijk, "Nanostructured materials for advanced energy conversion and storage devices," *Nature Materials*, vol. 4, no. 5, pp. 366–377, 2005.

[28] W. He, Y. Zhang, X. Zhang, H. Wang, and H. Yan, "Low temperature preparation of nanocrystalline Mn_2O_3 via ethanol-thermal reduction of MnO_2," *Journal of Crystal Growth*, vol. 252, no. 1–3, pp. 285–288, 2003.

[29] T. Nathan and A. Fauzi, "Electrochemical capacitor based on nano-sized Mn_2O_3 prepared by a novel solvolysis route," in *Proceedings of the 4th International Conference on Materials for Advanced Technologies (ICMAT '07)*, Singapore, July 2007, abstract no: K-7-PO12.

[30] T. Nathan, A. Aziz, A. F. Noor, and S. R. S. Prabaharan, "Nanostructured NiO for electrochemical capacitors: synthesis and electrochemical properties," *Journal of Solid State Electrochemistry*, vol. 12, no. 7-8, pp. 1003–1009, 2008.

[31] J.-H. Choy and Y.-S. Han, "Citrate route to the piezoelectric Pb(Zr,Ti)O_3 oxide," *Journal of Materials Chemistry*, vol. 7, no. 9, pp. 1815–1820, 1997.

[32] J.-L. Luche, "Sonochemistry: from experiment to theoretical considerations," in *Advances in Sonochemistry*, vol. 3, p. 85, JAI Press, Greenwich, Conn, USA, 1993.

[33] I. K. Gopalakrishnan, N. Bagkar, R. Ganguly, and S. K. Kulshreshtha, "Synthesis of superparamagnetic Mn_3O_4 nanocrystallites by ultrasonic irradiation," *Journal of Crystal Growth*, vol. 280, no. 3-4, pp. 436–441, 2005.

[34] C.-K. Lin, K.-H. Chuang, C.-Y. Lin, C.-Y. Tsay, and C.-Y. Chen, "Manganese oxide films prepared by sol-gel process for supercapacitor application," *Surface and Coatings Technology*, vol. 202, no. 4–7, pp. 1272–1276, 2007.

[35] H. Y. Lee, V. Manivannan, and J. B. Goodenough, "Electrochemical capacitors with KCl electrolyte," *Comptes Rendus de l'Académie des Sciences—Series IIC*, vol. 2, no. 11–13, pp. 565–577, 1999.

[36] S.-L. Kuo and N.-L. Wu, "Investigation of pseudocapacitive charge-storage reaction of $MnO_2 \cdot nH_2O$ supercapacitors in aqueous electrolytes," *Journal of the Electrochemical Society*, vol. 153, no. 7, pp. A1317–A1324, 2006.

[37] S. P. Cramer, F. M. F. De Groot, Y. Ma, et al., "Ligand field strengths and oxidation states from manganese L-edge spectroscopy," *Journal of the American Chemical Society*, vol. 113, no. 21, pp. 7937–7940, 1991.